ADVANCED MATERIALS TECHNOLOGIES
www.advmattechnol.de

# A Microfluidic Multiplex Sorter for Strain Development

*Chiara Leal-Alves, Sebastien Dumont, Zhiyang Deng, Sarah Alkhaldi, Ziuwin Leung, Michelle Oeser, and Steve C. C. Shih**

**Selecting strains with superior traits from strain improvement strategies is challenging, as it involves navigating the fitness landscape by applying selective pressures that drive variants from peaks of improvement to valleys over time. In recent years, the screening and selection is conducted via droplet microfluidic methods due to its high throughput capabilities. However, the oft-used binary strategy, targeting only the high levels of improved traits, may not reflect the overall enhancement. A multiplexed sorting method capable of applying an additional threshold to sort traits by phenotypic strength is reported. The novel approach uses a droplet-digital microfluidic sorter to screen different volumes of droplets using the same device design and sorting parameters. This method is used to sort glucoamylase enzyme mutants with two levels of activity (medium and high) from libraries of diastatic yeast that have been mutated with non-genetically modified techniques. Using the multiplex system, medium-performing strains with enhanced (up to 60%) fermentation kinetics in synthetic beverage media, which would have been missed with a binary screening approach, are identified. The multiplex sorting strategy efficiently finds strains with superior fermentation traits in the fitness landscape without requiring extensive screening rounds and mutations.**

## 1. Introduction

Strain improvement is a frequently used industrial method aimed to boost efficiency and yield of a microorganism to enhance their metabolic capacities. Current strain improvement methods revolve around generating genetic diversity through selection or adaptive laboratory evolution techniques. However, these methods do not always yield isolates with diverse phenotypes that meets the demands of industrial strains. Selection of isolates that have improved phenotypes depends on how we explore the fitness landscape.[1,2] Much like a rugged terrain with peaks and valleys, the fitness landscape illustrates the distribution of variants across different levels of fitness with peaks usually corresponding to high-level of the desired trait with valleys representing low-levels of it.[1,2] The selective pressures acting on strains can vary over time due to changes in environmental conditions. Variants frequently go through a temporal shift moving from peaks to valleys that could only be biologically relevant at a given time. A typical example is the evolution of an enzyme where variants can start high on the fitness landscape for native activity and then is found in the valleys of the fitness landscape at a different time point and again move toward the higher fitness later.[3,4]

To discern different functions or exploring different fitness landscapes has been traditionally performed by high-throughput screening and selection.[5–7] Using such a technique, generally involves a functional assay to identify a desired phenotype (e.g., cell growth or activity of a protein) and then selection for the top variants. Consequently, high throughput screening techniques have been extensively developed, with droplet microfluidics emerging as a leading cost-effective high-throughput approach.[8–10] Single cells are encapsulated in pico-nano liter droplets containing a chemical substrate that serve as a fluorescence or an absorbance reporter for the activity or function of the protein of interest.[11–13] This process is followed by incubation, to provide time to express the proteins of interest and to interact with their substrate. Finally, a sorting technique is implemented to obtain the most active based on their fluorescence or absorbance signals. With droplet microfluidics, the most common technique is to use dielectrophoretic (DEP) sorting, which is known to be able sort at 100 Hz to kHz range allowing to collect of at least $10^6$ cells per day.[12,14,15] This type of system is generally performed using binary selection criteria and has been applied to many different enzymatic directed evolution screens.[8,12,16] However, a binary search strategy, at a given time point, influences the effectiveness of finding the enzyme with the desired function. A more

C. Leal-Alves, Z. Deng, Z. Leung, S. C. C. Shih
Department of Electrical and Computer Engineering
Concordia University
Montréal, Québec H3G 1M8, Canada
E-mail: steve.shih@concordia.ca

C. Leal-Alves, Z. Deng, S. Alkhaldi, Z. Leung, S. C. C. Shih
Centre for Applied Synthetic Biology
Concordia University
Montréal, Québec H4B 1R6, Canada

S. Dumont, M. Oeser
Lallemand Inc
Montréal, Québec H4P 2R2, Canada

S. Alkhaldi, S. C. C. Shih
Department of Biology
Concordia University
Montréal, Québec H4B 1R6, Canada

The ORCID identification number(s) for the author(s) of this article can be found under https://doi.org/10.1002/admt.202401209



**DOI: 10.1002/admt.202401209**

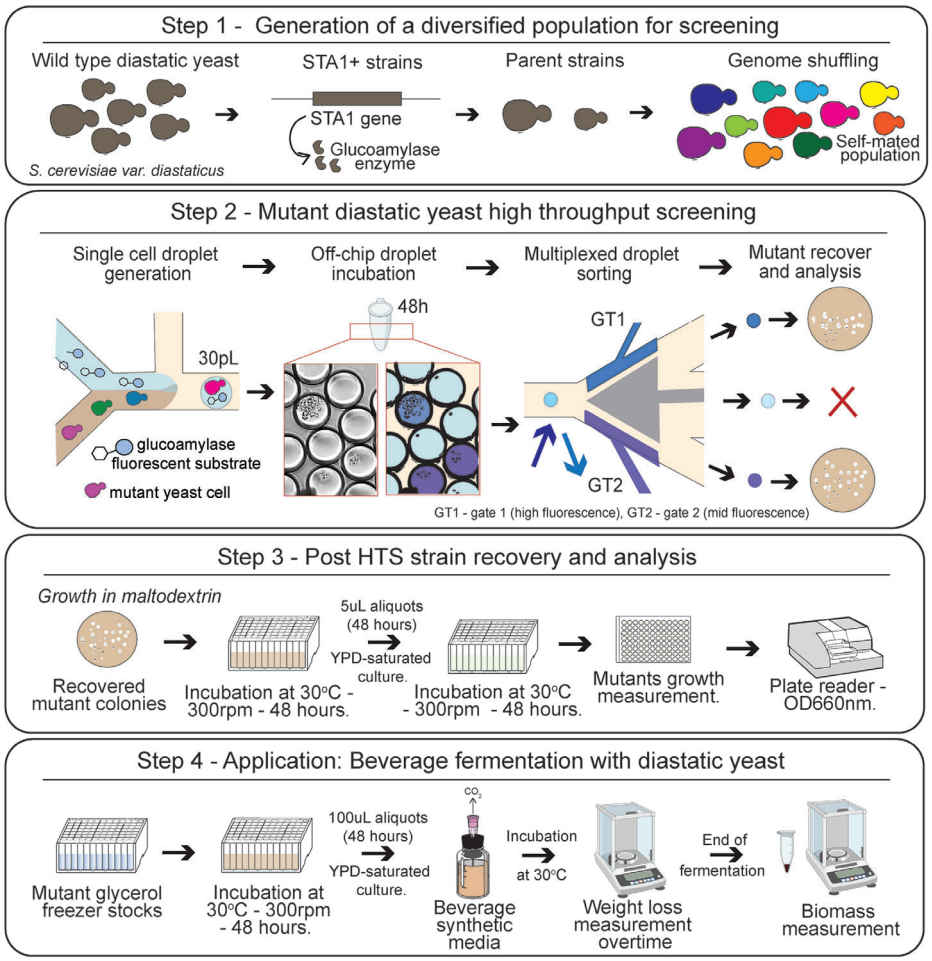


**Figure 1.** Development of a multiplex high throughput screening (HTS) workflow for strain improvement of *S. cerevisae var diastaticus* for beverage fermentation based on glucoamylase production. Step 1 – Generation of a diverse population library of STA1+ yeast strains through genome shuffling (self-mating) technique. Step 2 – High throughput screening of mutant yeast cells using a multiplex droplet microfluidic approach. First, yeast cells are encapsulated in droplets containing a fluorescent substrate for glucoamylase, then incubated off-chip for 48 h, and sorted based on two thresholds of fluorescence intensity to identify and to recover mutants with desired enzymatic properties. The sorted mutants are recovered in agar plates to collect individual colonies. Step 3 – Post high throughput screening analysis in maltodextrin, evaluating growth as a parameter. Cells are incubated for 48 h at 30 °C, and the best performant strains are selected for fermentation. Step 4 – The selected mutant strains are tested in a beverage fermentation setup. The fermentation process is monitored through weight-loss measurements (i.e., $CO_2$ release) and at the end of fermentation, biomass was assessed.

effective strategy is to perform a multiplexed technique that will sort protein function according to the strength of the phenotype. Although there have been efforts to integrate multiplex sorting with DEP,[11,17–19] these approaches face significant challenges as the number of sorting channels increases. The system's performance is highly dependent on the droplet's dielectric properties, the material in which the droplet is immersed, and the precise control of pressures, making it difficult to maintain consistency across multiple channels. Additionally, as we increase the number of sorting channels and electrodes, balancing the pressure and managing the arrangement of electrodes becomes increasingly difficult. This complexity is further compounded when variable droplet sizes are involved, which require frequent system redesign to ensure accurate sorting. Consequently, expanding the platform to accommodate diverse applications or organisms becomes a significant challenge, requiring constant reconfiguration to maintain precision and efficiency. Another option is to use electrostatic forces as a physical method to sort. The advantage with such sorters is that it uses much lower voltages (≈10 $V_{RMS}$)[20] and uses the electric field between the activated and ground electrodes to directly attract the droplet toward the desired channel.[21] Using such an approach does not require balancing of pressures or different potentials for sorting a wide range of droplet volumes. Currently, there are examples that use binary electrostatic sorters for enzyme screening,[20] finding tolerant strains,[22] and for antibody selection.[23] We expand on the previous work and implement a multiplexed electrostatic sorter to select for different phenotypic strengths. By using the electrostatic approach, we were able to design a more versatile device capable of sorting droplets ranging from 30 to 1000 pL without requiring any redesign.

**Figure 1** summarizes our pipeline employing our multiplex electrostatic droplet sorting system to sort model variant strains of *Saccharomyces cerevisiae*, specifically *S. cerevisiae var diastaticus*,

that secretes an industrial relevant glucoamylase enzyme. This yeast is frequently used in the beer and distilled beverage industries for its unique ability to ferment complex sugars that other yeast strains cannot metabolize. Thus, there is a strong interest in evaluating this strain for improved fermentation capability. In this work, we show that by sorting different strength phenotypes from a library of self-mated (>$10^6$ mutants) diastatic yeast, their catalytic performance of the mid-level strength strains was effectively enhanced more than the higher phenotypic strength yeast. We validated our workflow by demonstrating applicability for growth on starch-based media and further evaluated the top- and medium-performing strains in a fermentation setup cultured in a synthetic beverage media.[24]

## 2. Results and Discussion

### 2.1. Multiplex Electrostatic Sorter and Characterization

A key requirement for multiplex sorting based on multiple criteria is to design a device that will effectively drive the droplets into the selected channel. Patterned co-planar electrodes creates an electric field gradient between the activated and grounded electrode, directing the droplets toward this field, as shown in previous studies.[20–23,25] In our design, we expanded the typical binary sorting technique to create a symmetrical electrode geometry to be able to sort two different levels of fluorescence with a central channel for the nonselected "waste" droplets. The multiplex sorting device consists of three layers: electrode, dielectric and channel (Figure S1, Supporting Information). There are two inlets for the re-injected droplets and the spacer oil and three outlets for the sorted channels. As a first test, in the absence of the applied potential, we verified that all the droplets flowed into the central channel for different droplet volumes (30, 110, and 1000 pL) (Figure S2, Supporting Information). We re-injected each droplet population, varying the spacer oil flow rate from 100 to 600 nL $s^{-1}$, and as shown in **Figure 2A**, all the droplets were directed into the central channel regardless of their volumes for flow rates above 200 nL $s^{-1}$. These results also matched our simulations (Figure S3, Supporting Information), such that lower flow rates (<100 nL $s^{-1}$) do not provide sufficient pressure to consistently divert all droplets into the desired channel. Additionally, the increased resistance due to the droplet plugs, i.e., the 1 nL droplets in the main channel, often leads to droplets entering the nonselected channel.

Next, we investigated the functionality of our sorter by activating the electrodes such that the droplets are deflected toward the desired channel. We pulsed the potential to an electrode, either sorting electrode 1 (SE1) or sorting electrode 2 (SE2), as well as varied the oil flow rate to determine the number of successful re-injected droplets being sorted. Experimental outcomes demonstrate successful sorting across all droplet sizes and flow rates (>200 nL $s^{-1}$) at potentials above 105 $V_{RMS}$ (Figure 2B), which is consistent when compared to our previous electrostatic sorter[20] (12.5 $V_{RMS}$ and 50 nL $s^{-1}$). Our sorting technique is different compared to other works for multiplex sorting.[11,17,19] First, the electrodes can be aligned directly below the sorting junction and into the sorting channel. When a potential is applied to SE1 or SE2, the field laterally displaces the droplets directly into the sorting channel 1 (SC1) or sorting channel 2 (SC2), respectively (Figure S4, Supporting Information). Second, the electrode gaps between the ground and activated electrode are small (<25 mm), and this allows for a lower voltage (≈100 $V_{RMS}$) to be applied for sorting. Third, as droplets and plugs have different flow profiles in the channel. The uniform electrical field generated by the electrodes can intersect with the droplet or plug (Figure S5, Supporting Information), enabling sorting for both types of fluidic structures. Our simulations demonstrate that with a potential exceeding 105 $V_{RMS}$, the electrical field at mid-height of the channel, a field higher than $4 \times 10^5$ V $m^{-1}$ is achieved, which consequently, regardless of the droplet size, is sufficient for high efficiency sorting (Figure S4, Supporting Information). Therefore, a co-planar electrode design enables a robust and repeatable sorting method that does not require significant trial-and-error.

Using the optimized potential and re-injection flow rates, we evaluated the design for binary sorting using 1 mM fluorescein and phosphate buffered saline (PBS) droplets to quantify the efficiency and the sorting throughput (Figure S6, Supporting Information). We achieved high sorting efficiency (above 90.2%), a low false negative (Fn) rate (≈1.3%) and no significant difference in the sorting efficiency between channels (SC1 and SC2) across droplet sizes, similarly to our previous electrostatic droplet sorter (≈96% efficiency and ≈3% Fn, for 1 nL droplets at 7 Hz throughput).[20] For throughput of 30 pL droplets, we experimentally achieved screening rates of up to 160 Hz using our co-planar electrode system (Figure S7, Supporting Information). In addition, our multiplex sorter can efficiently collect two concentrations of fluorescein and nonfluorescein PBS droplets. We generated droplets for each volume and pooled them in a 1:1:5 ratio containing 0.1, 1 mM fluorescein, and blank PBS droplets, respectively (see Table S1, Supporting Information, droplet quantities). As shown in Figure 2C, sorting 30 pL volumes were very efficient for both concentrations (98.6% and 100% for 0.1 and 1 mM fluorescein, respectively). In fact, we were able to achieve a low false negative rate (≈3%), which means the sorting algorithm that we employed is an optimal method for sorting different fluorescent thresholds (Figure S8, Supporting Information). Similarly, we tested larger volumes (110 pL and 1 nL) and observed a very similar efficiency and even lower false negative rates, suggesting that our system is robust for sorting a range of droplet volumes. This discovery holds significant implications, particularly in the realm of droplet-based microfluidics where different organisms are encapsulated in a range of volumes from 4 to 1000 pL.[14,20,26–28] Numerous biological processes involve different droplet sizes and different operations, such as the fusion of droplets to establish reaction conditions[22,29–31] or incubation of droplets at higher than room temperatures.[10,32–34] These processes can alter droplet volumes and potentially complicating sorting processes. Our sorter eliminates the need for re-design and recalibration, distinguishing it from other types of sorters.[14,17,35]

### 2.2. Optimization of Cell Growth and Glucoamylase Activity from Diastatic Yeast

Enzymes that hydrolyze starch are essential in industrial processes such as alcoholic fermentation and food production.[36–38] Amongst the enzymes used for saccharification, glucoamylase

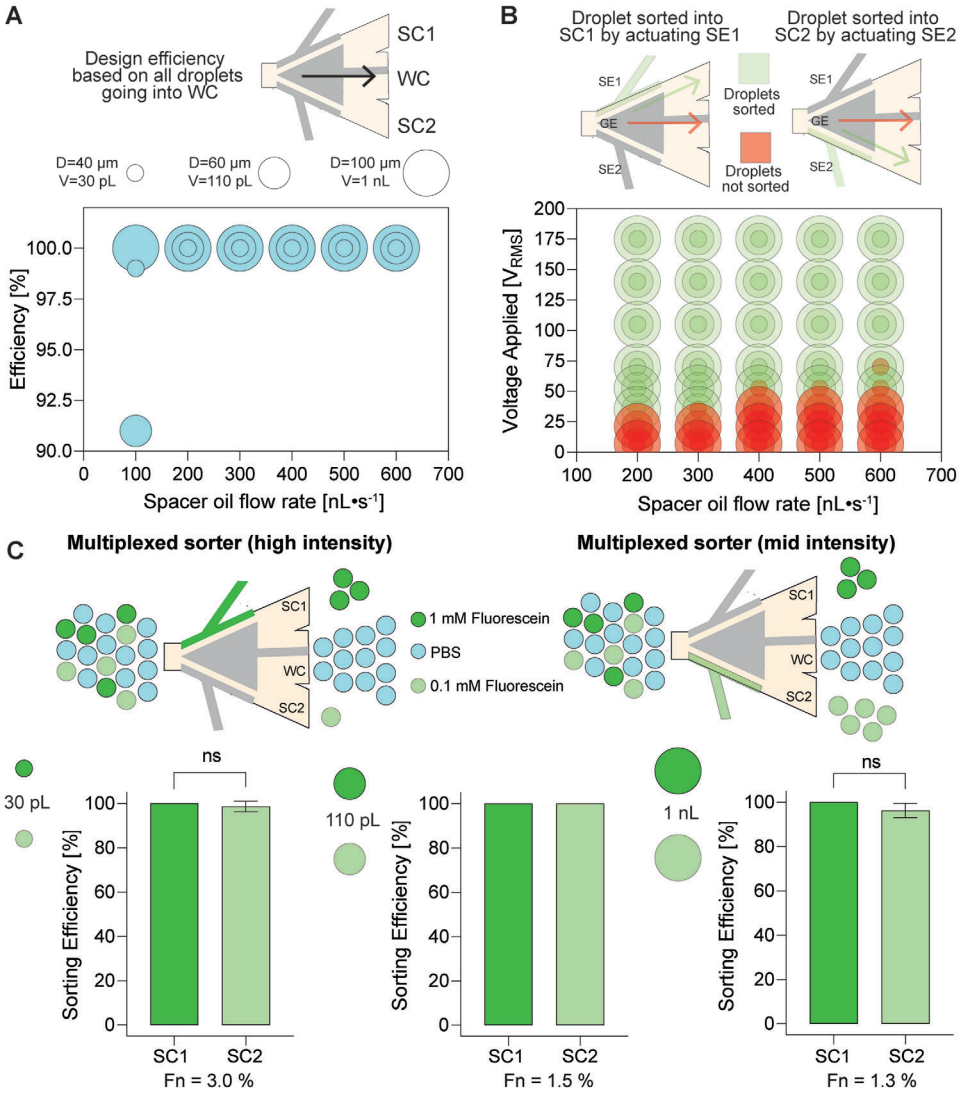


**Figure 2.** Assessment of our device's adaptability across varying droplet dimensions. The circles represent the different droplet sizes, and the throughput for all graphs was 100 Hz for 30 pL, 50 Hz for 110 pL, and 20 Hz for 1 nL. A) Characterization of spacer oil flow rates to direct all droplets into the waste channel without the activation of any electrode. Efficiency was measured by the amount droplets in the waste channel relative to the total amount of droplets. B) Characterization of the applied voltage's correlation with oil spacer flow rates when the sorting electrode is actuated with different $V_{RMS}$ potentials at 15 kHz for the three different droplet sizes. C) Multiplex sorting efficiency based on two thresholds of fluorescence intensity across various droplet sizes. The re-injected were part of a population containing PBS, 0.1 and 1 mM fluorescein. Efficiency is quantified by the proportion of fluorescent droplets in each respective sorting channel (SC1 or SC2) relative to the total number of droplets in that channel. False negatives (Fn) represent the percentage of fluorescent droplets in the waste channel. Error bars representing standard deviation $N = 7$, Unpaired $t$-test at 95% CI – $p$ values: 0.1234 (ns), 0.0332 (*), 0.0021 (**), 0.0002 (***), <0.0001 (****).

is frequently used in the industrial scale given their capabilities to release glucose units from starch molecules. In recent years, yeast strains have been engineered[39] to produce glucoamylase during fermentation because fermenting yeast from starch and dextrin represents a cost-effective method to produce ethanol and other metabolites. *Saccharomyces cerevisiae var. diastaticus*, usually seen as a brewing contaminant, has increased attention due to its potential for achieving higher ethanol concentrations and serving as a potential strain for carbohydrate-reduced and high-alcohol beverages.[40] Therefore, given the interest in these industrial arenas, we used our droplet microfluidic approach to screen mutant populations of two diastatic yeast strains (which we call, "Isolated Diastatic Yeast", IDY1 and IDY2) isolated from beverage industry to increase their ability to ferment starch and dextrin.

Screening enzyme activities has been demonstrated previously with absorbance[41,42] or fluorescence-based readouts.[8,20,35,43] Finding substrates to measure glucoamylase activity is challenging given that they have specific pH requirements to produce absorbance or fluorescence outputs. Currently, 4-nitrophenyl-$\beta$-d-maltoside (4-NPM) is a commonly used substrate to measure glucoamylase activity via absorbance,[44] and we tested 4-NPM as well as a glycosidase substrate 4-nitrophenyl-$\alpha$-d-glucopyranoside (4-NPG).[45,46] Only 4-NPM showed distinguishable signals for both isolated strains (IDY1 and IDY2) compared

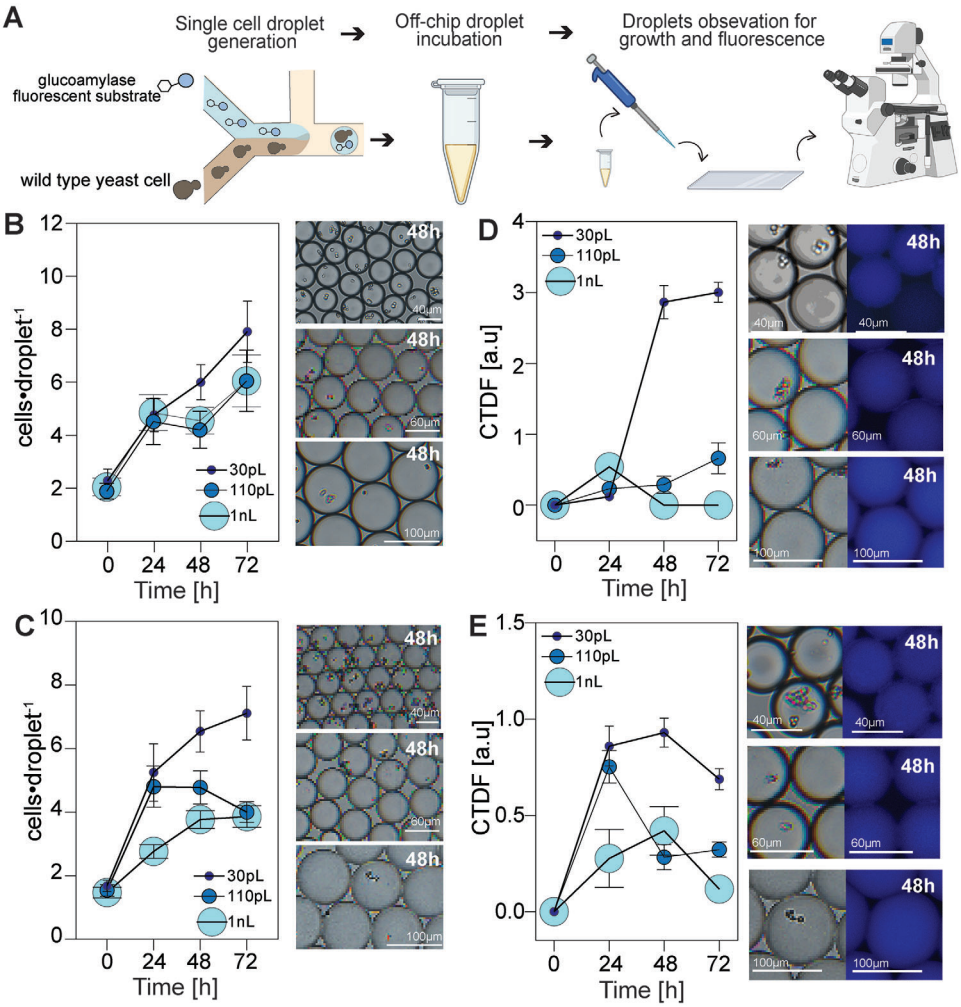


**Figure 3.** Characterization of droplet size and incubation time to screen diastatic yeast in droplets using glucoamylase activity as a metric. A) Pipeline to evaluate and to optimize growth conditions and glucoamylase activity in droplets. Single cell encapsulation in droplets with media (YPD) and fluorescence substrate, incubation off chip at 30 °C, and droplet observation using an inverted fluorescence microscope. Growth curves of B) IDY1 and C) IDY2 wild type in YPD droplets of varied volumes measured as number of cells per droplet. Evaluation of D) IDY1 and E) IDY2 wild type glucoamylase activity shown as fluorescence in different volumes of droplets over different incubation times. Error bars representing standard error $N > 9$.

to the negative control IY1 (isolated nondiastatic yeast) that does not secrete glucoamylase (Figure S9, Supporting Information). However, using an absorbance-based substrate is not favorable for high throughput screening of diastatic yeast as it requires a pH change (>10) to measure their activity, and at this high pH, it can lower their cell viability. Furthermore, droplet detection with absorbance substrates is not as sensitive as fluorescence techniques and usually require methods to increase the droplet path length for higher sensitivity.[22,42] Instead, we validated a fluorescence version, 4-methylumbelliferyl-$\alpha$-D-glucopyranoside (4-MUG-$\alpha$) that have been used yeast strains[47] (Figure S10, Supporting Information) and verified their activity under neutral and alkaline pH using a commercial glucoamylase. Although at alkaline pH there is higher measurable activity compared to the neutral, the fluorescence activity when incubated at neutral pH is distinguishable between the different concentrations of the added glucoamylase (Figure S11, Supporting Information). In addition, we evaluated the kinetics at pH 7.5 and observed a significant difference in the fluorescence of the isolated IDY1 and IDY2 strains versus the negative control (Figure S12, Supporting Information), confirming the suitability of this pH for our droplet system.

As far as we are aware this is the first report of work in which a droplet microfluidic activity screen was performed on diastatic yeast secreting glucoamylase. **Figure 3A** shows our workflow to systematically explore both diastatic yeast strains with YPD media at neutral pH and incubated with 4-MUG-$\alpha$ in different volume droplets (30, 110, and 1000 pL) up to 72 h and measured their droplet fluorescence using an imaging workflow (described in Figure S13 and Note S1, Supporting Information) and cell growth over time. As shown in Figure 3B, cell growth for IDY1 shows similar trends for all droplet volumes, with the 1 nL volume droplets growing at the fastest rate of ≈0.096 $h^{-1}$ (Table S2, Supporting Information). In contrast, for IDY2 (Figure 3C) only 30 pL significantly showed growth in comparison to the other volumes with a rate of ≈0.091 $h^{-1}$. Even though IDY1 and IDY2 were

both isolated from the beverage industry, they originate from different industrial settings. IDY2, from a low-sugar, low-alcohol setting, is less adaptable to higher sugar levels. While media concentration was consistent across droplet sizes (30, 110, and 1000 pL), the larger droplets had more sugar per cell, likely causing metabolic imbalances and reduced growth due to glucose repression in the IDY2 strains.[48–51] In contrast, IDY1, from a high-sugar, high-alcohol setting, is more robust and better suited for metabolizing elevated sugar levels, explaining its superior growth in larger droplets.

For fluorescence activity, IDY1 showed the highest glucoamylase activity (≈3 a.u.) when incubated in 30 pL droplets for 48 h (Figure 3D) and IDY2 showed similar trends as IDY1, but with lower peak fluorescence activity (≈1 a.u.) (Figure 3E). Therefore, we used 30 pL droplets and 48 h incubation time for the screening assay below due to the higher fluorescence and their faster throughput as well as optimization of cell growth.

### 2.3. Selecting and Evaluating Mutant Variants of Diastatic Yeast with Medium and High-Fitness Levels

Strict regulatory compliance and consumer preference has pushed the agro-food industries to use non-GMO mutagenesis techniques, such as mating and genome shuffling[52–54] to engineer libraries containing $>10^7$ variants. Selecting improved strains of a library of that size and genetic variability requires not only high throughput screening, but a better alternative for the selection approach.[7,55–59] When a trait undergoes directed evolution, it navigates a high-dimensional fitness landscape with the aim to find peaks representing optimal performance.[6,60] However, studies indicate that partitioning populations into sub-populations during screening for large libraries can expedite the discovery of desired traits faster than the typical binary approach.[61–65] Below we describe how a multiplex method of selection is particularly beneficial for non-genetically modified libraries,[60,66,67] aimed at improving the fermentation efficiency for glucoamylase.

We initially assessed the performance of our genome shuffled library in comparison to the wild-type (parental strain) by evaluating growth on maltodextrin (Figure S14, Supporting Information) and their enzyme activity (Figure S15, Supporting Information). The maltodextrin growth assays revealed no significant difference between the genome shuffled populations and the wild type. Although the IDY1 mutants exhibited a 1.5-fold increase in activity, the enzyme activity assays showed insignificant difference between the mutant populations and the wild type (Figure S15A, Supporting Information). These evaluations indicate minor differences between the mutant populations and their parental strains, poses a challenge for screening the genome shuffled populations for improved traits. To address this challenge and the fitness landscape, we used our multiplex device to sort the mutants into two distinct sub-populations.

Using the multiplex sorter, we encapsulated single mutant cells (via genome shuffling) diastatic yeast in YPD media and incubated in the dark with 4-MUG-$\alpha$ (the fluorescence substrate) in 30 pL droplets at 30 °C for 2 d. Representative distributions for the IDY1 (**Figure** 4A) and IDY2 (Figure 4B) strains after 2 d of culturing shows an expected Gaussian distribution. We

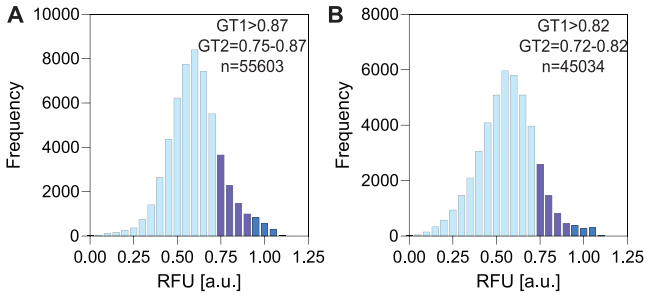


**Figure 4.** Histograms displaying droplet fluorescence used for multiplex sorting with different gates: high intensity (GT1) and medium intensity (GT2). A) IDY1 and B) IDY2 genome shuffled populations are single cell encapsulated in 30 pL droplets containing glucoamylase fluorescent substrate and incubated for 2 days at 30 °C.

screened ≈7 20 000 droplets at 160 Hz and sorted ≈1 08 000 droplets that we separated into two sub-populations gated as high-fluorescence intensity into gate threshold 1 (GT1 – dark blue), and midfluorescence intensity into gate threshold 2 (GT2 – purple).

We performed a quantitative comparison of the two selected subpopulations by picking 24 single colonies for each subgroup (Note S2, Supporting Information) and separated into single cultures. We measured enzyme activity and maltodextrin growth as both parameters are relevant in selecting improved strains for starch-based fermentation.[36] In maltodextrin, mid- and high-selected IDY1 mutants showed very little growth improvement compared to the wild-type, with only one and two high- and mid-strains respectively showing higher growth improvement after 24 and 48 h (Figure S16A, Supporting Information). However, for IDY2, every selected strain showed an improvement in growth, achieving on average 1.7 and 2.2 times more growth for mid- and high strains, respectively, than the wild type (parental strain) (Figure S16B, Supporting Information). The difference between the IDY1 and IDY2 growth rates could be due to the genome shuffling technique, such that IDY2 is starting with an enhanced growth phenotype in the maltodextrin and thus growing at a higher rate than IDY1 (Figure S14, Supporting Information).

The most significant difference was seen in the fold change enzyme activity data for IDY1 and IDY2, as shown in Figure S17A and S17B (Supporting Information), respectively. Using the selected gates, as expected, we observed the highest fold improvement for the high IDY1 selected strains (≈3.7 average) compared to the mid strains (≈1.2 average). However, for IDY2, 13 mid-selected strains and 7 high-selected strains showed improvement at the 24 and 48 h incubation points and with similar fold-change (≈2x improvement). This is a surprising result given that the selected high-variants are supposed to significantly outperform the wild-type (as shown from IDY1 and other studies[9,68]). From the growth and fluorescence data, we selected the most suitable mutants to be evaluated for fermentation efficiency using a lab-scale method intended to mimic industrial conditions (Figure S18, Supporting Information).[69,70]

In addition, we evaluated statistically their enzyme activity and maltodextrin growth in comparison to the wild type (mother strain). As shown in **Figure** 5A, all mutants except IDY1-H2 showed higher growth at both time points, however,

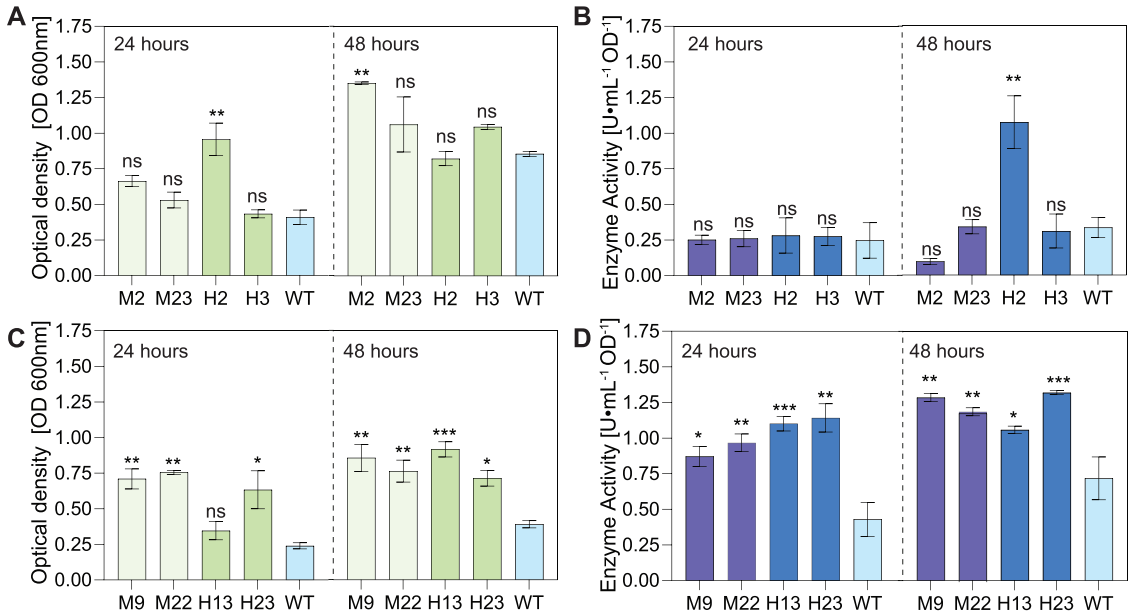


**Figure 5.** Evaluation of selected mutants in comparison to their wild type (mother strain). A) IDY1 and C) IDY2 mutant strains are grown in maltodextrin and measured by optical density after incubation at 30 °C for 24 and 48 h. B) IDY1 and D) IDY2 mutants showing glucoamylase activity using 4-MUG-$\alpha$ as the fluorescent substrate. M (Medium-level) and H (High-level) strains are mutants sorted into the medium (GT2) and high-level (GT1) sorting gates, respectively. Error bars representing standard error $N = 3$, one-way ANOVA at 95% CI compared to WT – $p$ values: 0.1234 (ns), 0.0332 (*), 0.0021 (**), 0.0002 (***), <0.0001 (****).

when analysing significant improvements, IDY1-H2 and IDY1-M2 showed ≈2.5 and ≈1.4 times more growth in maltodextrin in 24 and 48 h of incubation, respectively. For enzyme activity (Figure 5B), only IDY1-H2 showed statistical improvement over the wild type (approximately threefold improvement) after 48 h incubation. In contrast, for IDY2 (Figure 5C,D), all mutants showed statistically significant improvement in maltodextrin growth and enzymatic activity at both time points, except for IDY2-H13 at 24 h incubation, which shows similar growth in maltodextrin as the wild type (Figure 5C).

Genome shuffling of a strain with a heterozygous genome generates a genetically diverse population of variants derived from the parental strain, some of which may be enhanced over their parental strain for a trait of interest. However, other isolates of the population will be similar or worse than the parental strain for the trait of interest, necessitating an efficient sorting method for retrieving the desired isolates. Additionally, using a binary selection technique limits the landscape on finding a desired strain. Instead, dividing sorted strains into mid- and high-level of glucoamylase subpopulations using our multiplex sorter offers a broader landscape for screening those lacking genetic diversity. We examined a potential alternative, reducing the sorting threshold to include both high- and mid-level strain via binary sorting. Such a sorting experiment will sort more droplet samples; however, the probability to obtain a high- or a midlevel strain is not uniform (≈65% for the mid- and 35% for the high; Notes S2 and S3 and Table S3, Supporting Information). This creates a bias in the sorting and requires more sampling (at least 14 times more sampled strains) and testing compared to a multiplex screen to achieve the same confidence level of 95%. Based on a random sampling calculation,[71] the large sampling size as well as the nonuniform exploration of both fitness performing groups potentially leads to the loss of hits compared to simultaneous multiplexing them into two subpopulations (as in our study).

### 2.4. Fermentation of Mid- and High-Level Diastatic Yeast Mutants in Synthetic Beverage Media

It is well known that *Saccharomyces cerevisiae var. diastaticus* yeast have a well-established ability to produce higher ethanol content beverages,[37] carbohydrate-reduced beverages,[72] and facilitating starch-based one-pot fermentation for biofuels.[40] These types of yeast carry the STA genes that produce extracellular glucoamylase, which gives the yeast the ability to convert starch into sugars. Although this type of yeast is generally seen as a contaminant for the brewing industry, diastatic yeast can be useful for fermentation of malt or starch-based substrates. In the context of beverages, brewers may choose to use diastatic yeast to achieve a desired level of attenuation (i.e., sugars fermented into alcohol), to ferment complex substrates in applications where addition of exogenous enzyme is prohibited, or to create different beverage styles (such as those with lower final gravity). Using this as motivation, we evaluated the typical fermentation parameters: kinetics of the conversion, the yield, and their production levels.[73,74] Knowing such parameters can help provide decisions on strain selection based on performance of mutants relative to their parent strains. Hence, we conducted a fermentation assay with the selected mutant strains (Figure S18, Supporting Information) and evaluated the mass loss via $CO_2$ measurements (fermentation rate and yield) and their ability to produce ethanol in synthetic media (efficiency).

**Figure 6** shows the mass loss over time and the ethanol content at the end of 72 h fermentation experiment for the selected

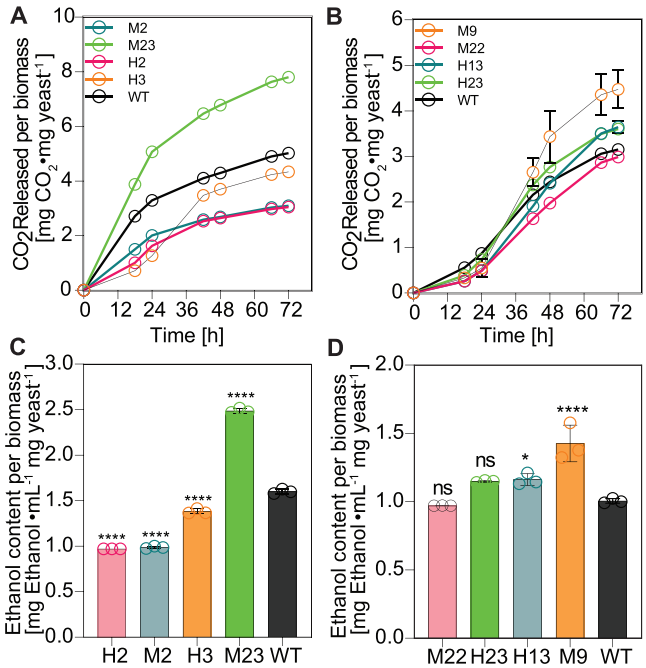


**Figure 6.** Evaluation of fermentation ability of the sorted mutant strains. A) IDY1 and B) IDY2 mutant's fermentation kinetics based on $CO_2$ released per biomass in a bioreactor using synthetic beverage media. Ethanol content normalized by dried biomass of C) IDY1 and D) IDY2 high and medium mutant strains from 72 h fermentation in synthetic media. Error bars representing standard deviation $N = 3$, one-way ANOVA at 95% CI compared to WT – $p$ values: 0.1234 (ns), 0.0332 (*), 0.0021 (**), 0.0002 (***), <0.0001 (****).

mutant strains. As shown in Figure 6A and Table S4 (Supporting Information), mutant strains showed a similar mass loss rate over time (i.e., fermentation rate) compared to the wild-type. There is only one mid-level sorted strain IDY1, M23 (green line), shows the highest mass loss of ≈7.8 mg of $CO_2$ per mg biomass at 72 h fermentation compared to the wild-type IDY1 strain (≈5.01 mg of $CO_2$ per mg biomass at 72 h fermentation). In addition, this mutant is the only one to show significant improvement over the wild type for ethanol content (Figure 6C). In comparison, IDY2, most of the strains undergo $CO_2$ mass loss, but two strains, M9 and H13, showed improvements in the mass loss rate (≈0.128 $h^{-1}$ – orange curve and ≈0.105 $h^{-1}$ – blue curve; Figure 6B) and achieve a higher loss of $CO_2$ than the wild-type strain after 72 h. Similarly, the two strains IDY2-M9, H13 (and IDY1-M23) exhibited a higher ethanol yield (normalized to biomass) compared to the wild-type (Figure 6D) with the top producers being mid-level sorted strains (IDY1-M23, IDY2-M9). We also compared their fermentation rate (Table S4, Supporting Information) and observed very similar rates between all the sorted strains and the wild-type. This observation is expected, given that there was no statistical difference between the genome shuffled populations in comparison to the mother strain (as shown in Figures S14 and S15, Supporting Information).

The observation that different mutant strains show different mass loss rates, yields, and production capabilities is not surprising; however, the outperformance of the medium strains is. The results show the importance of using a multiplex fluorescence screening method in selecting strains for complex traits like fermentation. Among the notable strains, two emerged from mid-level fluorescence selection (IDY1-M23, IDY2-M9), which would not have been selected if we used a binary screening approach. Selecting mid-level fluorescence strains avoids the growth trade-offs associated with high enzyme-expressing yeast, and the additional rounds of mutations or enhancement screening.[16,75,76] We hypothesize that the outperformance of mid-level strains can be attributed to a balance between enzyme production and metabolic burden, a well-studied phenomenon in heterologous protein production.[77–80] This concept, defined as the pressure on cellular resources caused by genetic manipulation and environmental factors, also applies to laboratory evolution techniques aimed at increasing native protein production or tolerance to harsh environments.[81–83] In our case, the high mutant strains exhibited lower fermentation efficiency, likely due to an increased metabolic burden from elevated glucoamylase expression. This burden could result from higher demands on ATP, increased consumption of amino acids for protein synthesis, and the redirection of cellular resources away from other essential processes like growth and energy generation (fermentation). As the cells prioritize glucoamylase production, their overall efficiency in fermentation may be compromised. In contrast, mid-level strains maintain a balance on enzyme secretion without overloading their metabolism, potentially leading to a better overall fermentation performance.

In summary, our approach identifies strains with optimal fermentation performance by balancing enzyme production and metabolic load, avoiding the inefficiencies that could have been seen in high-expression mutants. This method streamlines strain selection, reducing the need for further mutations or additional screening rounds while maintaining fermentation efficiency.

## 3. Conclusion

A novel high throughput (100 Hz) multiplex screening approach was developed using a droplet-digital, low-voltage, microfluidic sorter. The system was established by screening a genome and sorted them based on two levels of glucoamylase enzymatic activity. Given the ability of sorting into two populations (medium and high), we were able to decrease the sample size (≈14x) for post-analysis, which was previously not possible by just decreasing the threshold in binary sorters. Using this approach, we were able to select strains in the medium range with improved overall fermentation capability in beverage synthetic media. We believe our approach is the first step to accelerate the screening of more complex engineered microbes with varying activity that are used for many industrial applications.

## 4. Experimental Section

*Reagents, Materials, and Equipment*: Materials for fabrication and surface treatment of microfluidics devices included: transparent photomasks (Artnet Pro Inc., Bandon, OR), chromium-coated glass slides with AZ-1500 positive photoresist (Telic, Valencia, CA, USA), MF-321 developer (Kayaku Advanced Materials, Westborough, MA, USA), CR-4 chromium etchant (OM Group, Cleveland, OH, USA), AZ-300T photoresist stripper (Integrated Micro Materials, Argyle, TX, USA), silicon wafers (Silicon Valley Microelectronics Inc., Santa Clara, CA, USA), SU-8 series photoresists:

SU-8 5, SU-8 2035, SU-8 2075, and SU-8 developer (Kayaku Advanced Materials, Westborough, MA, USA), DI Water (resistivity of 15 MΩ $cm^{-1}$), acetone (cleanroom lab grade) and isopropanol (cleanroom lab grade) Sigma–Aldrich (Oakville, ON, CA), Chlorotrimethylsilane (Sigma–Aldrich – Oakville, ON, CA), Polydimethylsiloxane (PDMS) 184 Sylgard (Dow, Toronto, ON, CA), and 3M Novec 1720 (M.G. Chemicals, Burlington, ON, CA). Microfabrication equipment included: Harrick Plasma PDC-001 (Ithaca, NY, USA), Quintel Q-4000 mask aligner (Neutronix Quintel, Morgan Hill, CA), Laurell spin coater (model WS-650MZ-8NPPB, Laurell Technologies Corporation, North Wales, PA, USA), and mask aligner UV-KUB 3 (Kloe, Montpellier, France).

Materials for device operation included: Hamilton glass syringes (Reno, NV, USA), tubing and fittings (IDEX Health & Science LLC – Oak Harbor, WA), Optical fibers and bandpass filter (Thorlabs – Newton, NJ, USA), 3M Novec 1720 (M.G. Chemicals, Burlington, ON, CA), PEG fluoro-surfactant dissolved in HFE7500 (20 g of 5 wt%; Ran Biotechnologies, Beverly, MA, USA). All liquids were filtered using Nylon filter cartridges (0.22 µm, Millex GP, Millipore).

The hardware for sorting has been described previously by our group.[20,22,23,84] Equipment for device operation and automation hardware included: Low-pressure neMESYS pump system (Cetoni, Korbussen, DE), TREK high-voltage amplifier PZD700A (Advanced Energy Inc., Denver, CO, USA), 33210A Keysight function/arbitrary waveform generator 10 MHz (Keysight Technologies, Santa Rosa, CA, USA), GW Instek GPE-4323 Linear DC Power Supply with 4 Channels (GW Instek America Corp., Montclair, CA, USA), inverted microscope (Olympus IX73; Tokyo, Japan) mounted on a vibration-dampening bench (Thorlabs; Newton, New Jersey, USA), filter block (FOFMS-UV, Thorlabs; Newton, New Jersey, USA), multichannel LED light source MCLS 2073 (Ocean Optics; Orlando, FL, USA), bandpass filters (FB450-40 and FL457.9-10), fiber optics (FG105UCA – Ø 105 µm, FG200UEP – Ø 200 µm, and FG200LCC – Ø 200 µm) and UV LED light source (M375F2) (Thorlabs; Newton, New Jersey, USA), and a Hamamatsu ORCA-Flash 4.0 (Township, NJ, USA), and Flame spectrometer (Ocean Optics, Largo, FL). The above equipment list was summarized in Table S5 (Supporting Information) with their connectivity between the components shown in Figure S19 (Supporting Information). The software is available in the Github repository (https://bitbucket.org/shihmicrolab/f_ahmadi_2023_uflowcontrol).[23]

Fluorescein, yeast culture reagents, 4-methillumbeliferyl fluorescent substrates, 4-nitrophenyl absorbance substrates, and other general-use chemicals and kits were purchased from Sigma–Aldrich (St. Louis, MO) unless specified otherwise.

*Glucoamylase Enzymatic Assay and Maltodextrin Growth*: *Saccharomyces cerevisiae var. diastaticus* STA1+ strains (IDY1 and IDY2) isolated from beverage industry, *Saccharomyces cerevisiae* STA1- strain (IY1; negative control), recombinant *Saccharomyces cerevisiae* (IRY1) containing a heterologous glucoamylase gene (positive control) were obtained from Lallemand Inc.

To measure glucoamylase activity, three different substrates were used: 4-nitrophenyl $\beta$-D-maltoside (4-NPM), 4-nitrophenyl $\alpha$-D-glucopyranoside (4-NPG-), and 4-methylumbelliferyl-$\alpha$-D-glucopyranoside (4-MUG-$\alpha$). Prior to an end-point measurement, yeast strains were cultured on yeast peptone dextrose (YPD broth) for 48 h at 30 °C and shaking at 300 rpm. The optical density at 600 nm was measured using a Tecan Sunrise microplate reader (Tecan, Salzburg, Austria), and the enzyme activity was measured in 96-well plates containing 50 µL of the enzyme substrate (2 mM final concentration) and 50 µL of the supernatant cell culture, followed by incubation at 30 °C for 2 h, and the addition of stop buffer (pH 11). Absorbance activity (for the nitrophenyl substrates) was measured at 405 nm in a Tecan Sunrise microplate reader and the activity was calculated based on the extinction coefficient of 4-nitrophenyl ($\varepsilon$ = 18 000 $M^{-1}$ $cm^{-1}$) and Beer's Law equation. The fluorescence ($I_{ex}$ = 360 nm, $I_{em}$ = 450 nm) was measured in a CLARIOstar Plus (BMG LABTECH, Ortenberg, Germany), and activity was calculated using a methylumberiferyl standard curve.

To evaluate the pH dependence of the fluorescence substrate, the activity curve of commercial *Aspergillus niger* amyloglucosidase enzyme using the 4-MUG-$\alpha$ substrate at pH 7.5 and 11 at the same volumes and concentrations as above was measured. For evaluation of enzyme activity during cell growth, the yeast strains IDY1, IDY2, and IY1 were grown overnight at YPD broth at 30 °C and shaking at 300 rpm. In a 96-well plate, 20 µL of the culture was added to 150 µL of YPD broth and to 30 µL of 4-MUG-$\alpha$ (2 mM final concentration). The solution was incubated at 30 °C and 200 rpm, and the fluorescence ($I_{ex}$ = 360 nm, $I_{em}$ = 450 nm) was measured every 1 h for 15 h in the CLARIOstar Plus.

To measure the growth on maltodextrin, the strains (IDY1, IDY2, IY3, and IRY1) were grown for 48 h in YPD broth at 30 °C and shaking at 300 rpm. Five microliters of the culture was added to 1 mL of maltodextrin media (2 g $L^{-1}$ yeast extract, 4 g $L^{-1}$ bacto™ peptone, and 20 g $L^{-1}$ maltodextrin), and optical density at 600 nm was measured at 24 and 48 h.

*Genome Shuffling Library Generation and Culture*: Sporulation of the two diastatic strains IDY1 and IDY2 was induced by inoculation of saturated cultures into sporulation medium (1 g $L^{-1}$ yeast extract, 10 g $L^{-1}$ potassium acetate, 0.5 g $L^{-1}$ glucose) with a starting OD600 of 0.3 followed by incubation for 5 days at 23 °C with 150 rpm agitation. Sporulation was confirmed by microscopic inspection. Spores were prepared according to the ether-zymolyase ascospore technique.[85] Spores were then incubated in a small volume (≈50 µL) of YPD with 2% glucose at 30 °C overnight. The culture was then pitched in 5 mL of 2% YPD medium and incubated at 30 °C overnight. Multiple single-use freezer stocks were produced by adding glycerol (25% final) to the saturated YPD culture.

*Microfluidic Device and Fabrication*: The devices were fabricated by photolithography and soft-lithography methods. Photomasks were designed using AutoCAD 2022 and printed (Artnet Pro Inc., Bandon, OR). Different channel heights and widths were patterned onto a 100 mm Si-wafer that were cleaned with acetone, isopropyl alcohol, and DI water, followed by treatment under plasma oxygen for 2 min 30 s prior to use. SU-8 2075 was used for 75 µm channel heights and widths and followed manufacturer's instructions for spin-coating (10 s – 500 rpm, 30 s – 2500 rpm, and 10 s – 500 rpm), baking, and exposure time. SU8-2035 was used for 35 µm channel heights and widths and followed manufacturer's instructions for spin-coating (10 s – 500 rpm, 30 s – 3250 rpm, and 10 s – 500 rpm) and 50 µm channel heights and widths and followed manufacturer's instructions for spin-coating (10 s – 500 rpm, 30 s – 2500 rpm, and 10 s – 500 rpm) baking and exposure time. The resulting master mold was exposed to chlorotrimethylsilane vapor deposition in a desiccator for 45 min. Next, PDMS (1:10 w/w ratio curing agent to prepolymer), degassed and poured over the mold and left to cure in an oven (65 °C, 2 h). PDMS layers were cut to size with an X-Acto knife. Inlets and outlets were made using 0.75 mm biopsy punchers (World Precision Instruments, FL, USA), and were fitted with 1/32″ OD tubing after which the PDMS was carefully washed with isopropyl alcohol, DI water, air dried, and cleaned with tape to remove dust before device assembly. The PDMS channel layer and a glass slide were treated with oxygen plasma for 45 s and bonded together and baked at 90 °C for 30 min. Device channels were then treated with Novec 1720 fluorosilane polymer surfactant, followed by a baking step of 160 °C for 30 min.

The co-planar sorter device consisted of an electrode and dielectric layer prior to incorporating a channel layer, as previously reported.[20,22,23,25] Briefly, chromium-coated 50 × 75 mm glass slides (Telic, Valencia, CA, USA), with S1811 positive were UV exposed (7 s at 38–50 mW $cm^{-2}$), then developed in MF-321 developer, etched with CR-4 chromium etchant, and stripped with AZ-300T photoresist stripper. For the dielectric layer, the resulting patterned electrode substrate was placed under plasma oxygen (Harrick Plasma PDC-001, Ithaca, NY) for 2 min, after which they were immediately spin coated with an SU-8 5 layer (10 s – 500 rpm, 30 s – 2000 rpm, and 10 s – 500 rpm), soft baked, and exposed to a patterned mask. After post-baked, substrates were developed with SU8 developer, rinsed with isopropyl alcohol and DI water, and underwent a hard baked cycle (200 °C, 30 min, gradual ramping) to obtain a 7 µm thick layer.

For the channel layer, SU-8 2075 was spin coated (10 s – 500 rpm, 30 s – 2000 rpm, and 10 s – 500 rpm) to obtain a 100 µm thick layer, followed by a baking and exposure cycle according to the manufacturer's datasheet. A second layer (for the emission optical fiber only) containing SU-8 2075 was spin coated on top of the nondeveloped first layer (10 s – 500 rpm,

30 s – 2000 rpm, and 10 s – 500 rpm) to obtain a 100 µm thick layer. After pre-exposure bake, the second layer mask was aligned and exposed (UV-KUB 2, Kloé, France), followed with baking and development according to the manufacturer's datasheet. The master mold was silanized and used for PDMS creation following the protocol above. The PDMS channel containing the sorter channel was manually aligned with the dielectric coated electrodes using an inverted microscope 4X (Olympus IX73; Tokyo, Japan). Device channels were then treated with Novec 1720 fluorosilane polymer surfactant. Two flat cleaved multimode optical fibers were prepared for droplet excitation (100 µm core, 0.22 N.A.) and detection (200 µm core, 0.49 N.A.) (Thorlabs, NJ, US). Fibers were fixed with Kapton tape directly on the device. To collect droplets from the sorter, three pipette tips (200 µL) were positioned at the outlets and 30 µL HFE oil was added before running the system.

*Sorter device operation and validation*: Gastight 500 mL glass syringes were prepared with fittings and tubing as reported previously by the group.[20,22,25,84] The syringe for droplet reinjection were set up with a 1/32″ OD, 0.381 mm ID PEEK tubing. All other syringes had a 1/32″ OD, 0.127 mm ID tubing. Syringes were installed on a low-pressure neMESYS pump system (Cetoni, Korbussen, DE). The sorting device with installed optical fibers was fixed in a 3D-printed holder (Figure S20, Supporting Information) and clamped in place with a pogo pin PCB providing contact with the electrode pads. The holder base plate fits in the scanning stage (XYZ Tango, Marzhauser, Wetzlar, DE) of an inverted epi-fluorescence microscope (Olympus IX78, Olympus, Montreal, Québec, CA). Next, the SMA end of the excitation fiber was coupled to a 500 nm short-pass filter in an in-line fiber optic filter mount (Thorlabs, NJ, US), connected to a high power (1 mW) 470 nm fiber coupled LED light source. The SMA end of the emission fiber was coupled to a portable mini-spectrometer (FLAME-S UV–VIS, Ocean Insight, NY, USA). The flow inside the microfluidic channel was observed under a 4x or 10x objective under bright-field illumination. The spectrometer, pressure driven fluid flow and electrode actuation were controlled using an in-house automation system and graphical user interface.[23]

The multiplex sorter design was evaluated by generating different droplets volumes (30, 110 pL, and 1 nL) from a droplet generator (Figure S2, Supporting Information), respectively and reinjecting them into the sorter by changing the spacer oil flow rate (100–700 nL $s^{-1}$) with no electrode actuation. The design efficiency was calculated by dividing the number of droplets flowing into the waste channel by the total number of droplets generated.

To optimize voltage conditions, the different droplet sizes and spacer oil flow rates were evaluated by a two-sorting experiment (droplet flowing into the sorting channels, SC1 and SC2 or flowing into the waste channel, WC). Both the applied AC signal amplitude (15 kHz, sine wave, 7–175 $V_{RMS}$, 8 levels) and the spacer oil speed (200–600 nL $s^{-1}$, 5 levels) were varied, however, the droplet re-injection rate was kept the same (30 pL – 100 Hz, 110 pL – 50 Hz, and 1 nL – 20 Hz). Droplets were sorted by actuating the sorting electrodes SE1 or SE2, and the sorting response was measured by droplets moving toward the activated sorting channel, and the droplet travel time and actuation time were experimentally recorded. For data analysis, images were recorded using a Hamamatsu Flash LT+ 4.0 camera.

To validate autonomous sorting, the sorting efficiency was measured for all droplet sizes (30, 110 pL, and 1 nL). A mixed population of 1 mM fluorescein and PBS droplets were injected into the sorter (for 30 pL: 4 nL $s^{-1}$ droplet flow rate, 400 nL $s^{-1}$ spacer oil flow rate, 0.4 ms travel time and 10 ms actuation time; for 110 pL: 6 nL $s^{-1}$ droplet flow rate, 400 nL $s^{-1}$ spacer oil flow rate, 0.4 ms travel time and 20 ms actuation time; for 1 nL: 25 nL $s^{-1}$ droplet flow rate, 500 nL $s^{-1}$ spacer oil flow rate, 0.4 ms travel time and 30 ms actuation time). The fluorescence intensity was measured using the optical fibers from the devices and an in-house program will use the intensity to route the droplets into one of the two sorting channels (15 kHz sine wave and 105 $V_{RMS}$). The efficiency was measured by calculating the true positive percentage of fluorescent droplets being sorted into the sorting channels (see Equation 1) and the false positives (Equation 2). False negative percentage was determined by the percentage of fluorescent droplets into the waste channel based on the Equation (3). Images of the droplets in the sorting channels and waste channels were recorded using a Hamamatsu Flash LT+ 4.0 camera. Moreover, to validate the multiplex autonomous sorter, efficiency was measured following the same protocol above, except using a mixed population of PBS, 1 mM, and 0.1 mM Fluorescein droplets.

$$\textit{True positive}\ \ (\%) = \left(1 - \frac{(TSD - FD)}{TSD}\right) \times 100 \tag{1}$$

$$\textit{False positive}\ \ (\%) = \frac{(TSD - FD)}{STSD} \times 100 \tag{2}$$

where TSD is the total number of sorted droplets into the sorting channel, and FD is the number of sorted droplets that are fluorescent.

$$\textit{False negative}\ \ (\%) = \left(\frac{FD}{TWD}\right) \times 100 \tag{3}$$

where TWD is the total number of droplets into the waste channel, and FD is the number of sorted droplets that are fluorescent.

*Microscale Culture and Screening of S. cerevisiae var. diastaticus*: Parental strains of IDY1 and IDY2 were inoculated in YPD broth at 30 °C with shaking at 200 rpm overnight. The cultures were sonicated and washed using PBS by centrifugation and repeated three times. The final pellet was resuspended into 2x YPD broth (buffered at pH 7.5). Since the cell solution would be co-encapsulated (1:1 ratio) with the substrate solution, the OD600 were adjusted for twice the single cell droplet ratio based on Poisson distribution ($\lambda = 0.3$) for the different droplet sizes (30 pL – $2 \times 10^7$ cells $mL^{-1}$, 110 pL – $5 \times 10^6$ cells $mL^{-1}$, 1 nL – $6 \times 10^5$ cells $mL^{-1}$). Once cell concentration was adjusted, 10 %(w/w) Bovine serum albumin was added to the cell solution. The cell solution in 2x YPD broth were co-encapsulated with 4 mM (2 mM droplet concentration) 4-MUG-$\alpha$ (buffered in 0.1 M phosphate buffer pH 7.5) in the T-junction droplet generators (for volumes 30, 110 pL, and 1 nL) using 2% fluorosurfactant in HFE7500 oil, and the droplet generation was monitored and measured using Fiji (Image J) to form the desired droplet sizes (Figure S2, Supporting Information). Droplets were collected into a PCR tube with 50 µL of 2% fluorosurfactant in HFE7500 oil and incubated at 30 °C in the dark for 72 h. Fluorescence and bright field images were taken every 24 h to measure cell growth and glucoamylase enzyme activity.

Cell growth was measured by counting the number of cells inside the droplets, and glucoamylase activity was measured based on 4-MU fluorescence. The fluorescence intensities were measured using Fiji (image J) based on previously reported technique[86] with modifications (see Figure S13 and Note S1, Supporting Information, for reference). To measure fluorescence intensity in droplets and correction for fluorescent background signals, the freehand ROI tool was used to outline the desired regions. Subsequently, the area was measured, density was integrated, and the mean gray value was selected. To calculate the corrected total droplet fluorescence (CTDF), Equation (4) has been used and the results have been averaged based on eight data points.

$$CTDF = \frac{DF}{DA \times Mean\ BR} - \frac{DF_{t0}}{DA_{t0} \times Mean\ BR_{t0}} \tag{4}$$

where DF is the integrated density of the droplets that refers to the sum of the values of all the pixels in a selected area or region of interest (ROI) in an image, DA is the droplet area, and Mean BR is the mean fluorescence of background readings. $DF_{t0}$, $DA_{t0}$, and Mean $BR_{t0}$ denote the same measurements, but they were taken immediately after droplet generation and before incubation.

*Mutant Droplet Generation, Sorting, and Recovery*: The genome-shuffled mutant population of *S. cerevisiae var. diastaticus* strains (IDY1 and IDY2) was prepared and encapsulated in droplets as the protocol above for 30 pL droplets, collected in PCR tubes and incubated for 48 h. After incubation, the droplets were re-injected into the sorter through a flow rate of 3 nL $s^{-1}$ and spacer oil flow rate of 300 nL $s^{-1}$. The fluorescence of the population was measured and graphed into a histogram to set up the sorting gates (gate-SC1 – high fluorescence 95th percentile, and gate-SC2 – mid

fluorescence 85th percentile). Each gate was selected to sort droplets into two separated channels (SC1 and SC2) by actuating (15 kHz sine wave and 105 $V_{RMS}$) the sorting electrodes SE1 and SE2, respectively. The droplets were collected by pipetting the top layer of the emulsion from the pipette tips positioned at the outlets. From sorted populations (high and mid fluorescence), 5 µL aliquots were taken and diluted into 50 µL of YPD broth and plated on YPD agar plates, the remaining emulsion was pipetted in YPD broth and grew overnight to generate subpopulation glycerol stocks. The plates were incubated at 30 °C for 48 h, and several colonies were taken for post-sorting mutant analysis such as fold improvement in enzyme activity (Equation 5) and growth (Equation 6) on maltodextrin as described in the macroscale culture section.

$$\textit{Enzyme Activity Fold Improvement} = \frac{\textit{Mutant Enzyme Activity}\left(\frac{U}{mL \cdot OD}\right)}{\textit{Wild type Enzyme Activity}\left(\frac{U}{mL \cdot OD}\right)} \quad (5)$$

$$\textit{Maltodextrin growth Fold Improvement} = \frac{\textit{Mutant OD}}{\textit{Wild type OD}} \quad (6)$$

*Fermentation Evaluation of Mutant Strains*: Fermentation improvement was evaluated through $CO_2$ release measured by weight loss following the previously described method[24] with modifications. A preculture of the mutant strains and the wild type were done in YPD broth for 48 h with shaking at 300 rpm and incubated at 30 °C. Hundred microliters of the inoculum was added to 3 mL of synthetic medium (125 g $L^{-1}$ maltose, 60 g $L^{-1}$ maltodextrin, 1 mL ethanol, 1.25 mL (50% in water) glycerol, 3 mL 85% lactic acid, 2 g $L^{-1}$ yeast extract, 6.4 g $L^{-1}$ bactopeptone, pH adjusted to 5.9 and 25 mg $mL^{-1}$ chloramphenicol). The synthetic media was added to 6 mL mini vials (VWR, Mississauga, ON) and sealed with rubber caps pierced with needles for gas exchange. The initial weight for each vial containing media and inoculum was recorded using a precision scale and set as time = 0. The samples were shaken for 5 min at 180 rpm to ensure proper mixing of cells with the medium. Subsequently, they were incubated without agitation at 20 °C for 22 h, followed by an increase in temperature to 30 °C until the end of the fermentation. Weight loss was measured at 0, 18, 24, 42, 48, 66, and 72 h (time intervals and fermentation was considered complete at 72 h (final mass loss point)). Additionally, the dry biomass weight was measured by pelleting the cells and drying them at 60 °C overnight. Calculations were conducted using the equations shown in Note S4 (Supporting Information).

*Modeling and Data Analysis*: Data and statistical analysis were performed using GraphPad Prism v10.2.3. Image analysis and droplet sizes calculations were done using Fiji (Image J). The applied electrical signal was measured using an oscilloscope. The graphical figures were generated with Adobe Illustrator and Biorender. 2D Flow velocity and 3D electrical field simulations were performed with COMSOL Multiphysics v5.4 with modeling parameters described in Table S6 (Supporting Information). All in-house codes were previously described by the group.[20,23]

*Statistical Analysis*: Statistical analysis was performed using Prism v10.2.3 (GraphPad). For Figure 2, Figures S6 and S15 (Supporting Information), unpaired *t*-test was performed at 95% CI with $n = 7$ replicates for Figure 2, $n > 3$ for Figure S6 (Supporting Information), and $n = 3$ for Figure S15 (Supporting Information), *p*-values included in the captions. For Figures 5 and 6, Figures S9, S10, and Table S4 (Supporting Information), we performed One-way ANOVA at 95% CI, with $n = 3$ replicates for Figures 5 and 6, Figures S9, S10, and Table S4 (Supporting Information), *p*-values included in the captions.

## Supporting Information

Supporting Information is available from the Wiley Online Library or from the author.

## Acknowledgements

The authors thank the Natural Sciences and Engineering Research Council (NSERC), the Canadian Foundation of Innovation (CFI), and Lallemand Inc. for funding. C.L.A. thanks the FRQNT B2X for graduate funding, and along with Z.D. thank NSERC CREATE SynBioApps program for graduate funding. C.L.A., Z.D., and Z.L. thank the Concordia University Department of Electrical and Computer Engineering for FRS funding and the Biology Department for academic resources. S.C.C.S. thanks Concordia for a University Research Chair.

## Conflict of Interest

The authors declare no conflict of interest.

## Author Contributions

C.L.A. designed and built all the devices, conducted the droplet microfluidic and strain improvement experiments. C.L.A. and S.C.C.S. analyzed the data and organized the data/figures. C.L.A., S.D., M.O., and S.C.C.S. designed the yeast culturing experiments. S.D. and M.O. generated the genome shuffled (self-mating) population. Z.D. aided with the design and fabricated the microfluidic devices. S.A. helped in the fermentation assays. C.L.A. and Z.L. conducted the COMSOL simulations. C.L.A. and S.C.C.S. wrote the manuscript, and all authors reviewed the final version of the manuscript before submission.

## Data Availability Statement

The data that support the findings of this study are available from the corresponding author upon reasonable request.

## Keywords

droplet microfluidics, genome shuffling, high throughput screening

Received: July 25, 2024
Revised: October 7, 2024
Published online: November 11, 2024

[1] P. A. Romero, F. H. Arnold, *Nat. Rev. Mol. Cell Biol.* **2009**, *10*, 866.
[2] M. S. Packer, D. R. Liu, *Nat. Rev. Genet.* **2015**, *16*, 379.
[3] B. L. Wang, A. Ghaderi, H. Zhou, J. Agresti, D. A. Weitz, G. R. Fink, G. Stephanopoulos, *Nat. Biotechnol.* **2014**, *32*, 473.
[4] H. Jacquier, A. Birgy, H. Le Nagard, Y. Mechulam, E. Schmitt, J. Glodt, B. Bercot, E. Petit, J. Poulain, G. Barnaud, P.-A. Gros, O. Tenaillon, *Proc. Natl. Acad. Sci. U. S. A.* **2013**, *110*, 13067.
[5] R. J. McLure, S. E. Radford, D. J. Brockwell, *Trends Chem.* **2022**, *4*, 378.
[6] A. Jain, S. Stavrakis, A. deMello, *Curr. Opin. Biotechnol.* **2024**, *87*, 103097.
[7] W. Zeng, L. Guo, S. Xu, J. Chen, J. Zhou, *Trends Biotechnol.* **2020**, *38*, 888.
[8] T. Beneyton, S. Thomas, A. D. Griffiths, J. M. Nicaud, A. Drevelle, T. Rossignol, *Microb. Cell Fact.* **2017**, *16*, 18.
[9] S. L. Sjostrom, Y. Bai, M. Huang, Z. Liu, J. Nielsen, H. N. Joensson, H. A Svahn, *Lab Chip.* **2014**, *14*, 806.
[10] I. C. Clark, P. Mudvari, S. Thaploo, S. Smith, M. Abu-Laban, M. Hamouda, M. Theberge, S. Shah, S. H. Ko, L. Pérez, D. G. Bunis, J. S. Lee, D. Kilam, S. Zakaria, S. Choi, S. Darko, A. R. Henry, M. A. Wheeler, R. Hoh, S. Butrus, S. G. Deeks, F. J. Quintana, D. C. Douek, A. R. Abate, E. A. Boritz, *Nature.* **2023**, *614*, 318.

[11] W. Verbist, J. Breukers, S. Sharma, I. Rutten, H. Gerstmans, L. Coelmont, F. Dal Dosso, K. Dallmeier, J. Lammertyn, *Lab Chip.* **2024**, *24*, 2107.
[12] E. J. Medcalf, M. Gantz, T. S. Kaminski, F. Hollfelder, *Anal. Chem.* **2023**, *95*, 4597.
[13] E. Lebrun, V. Shenshin, C. Plaire, V. Vigneres, T. Pizette, B. Dumas, J.-M. Nicaud, G. Mottet, *Lab Chip.* **2023**, *23*, 3487.
[14] A. Isozaki, A. Isozaki, Y. Nakagawa, M. H. Loo, Y. Shibata, N. Tanaka, D. L. Setyaningrum, J. W. Park, Y. Shirasaki, H. Mikami, D. Huang, H. Tsoi, C. T. Riche, T. Ota, H. Miwa, Y. Kanda, T. Ito, T. Ito, K. Yamada, O. Iwata, K. Suzuki, S. Ohnuki, Y. Ohya, Y. Kato, T. Hasunuma, T. Hasunuma, S. Matsusaka, M. Yamagishi, M. Yazawa, S. Uemura, et al., *Sci. Adv.* **2020**, *6*, eaba6712.
[15] S. A. Johansson, T. Dulermo, C. Jann, J. D. Smith, A. Pryszlak, G. Pignede, D. Schraivogel, D. Colavizza, T. Desfougères, C. Rave, A. Farwick, C. A. Merten, K. R. Roy, W. Wei, L. M. Steinmetz, *Lab Chip.* **2023**, *23*, 3704.
[16] R. G. Rosenthal, X. D Zhang, K. I. Đurđić, J. J. Collins, D. A. Weitz, *Angew. Chem. Int. Ed. Engl.* **2023**, *62*, e202303112.
[17] O. Caen, S. Schütz, M. S. S. Jammalamadaka, J. Vrignon, P. Nizard, T. M. Schneider, J.-C. Baret, V. Taly, *Microsyst. Nanoeng.* **2018**, *4*, 33.
[18] D. Frenzel, C. A. Merten, *Lab Chip.* **2017**, *17*, 1024.
[19] A. Isozaki, D. Huang, Y. Nakagawa, K. Goda, *Microfluid. Nanofluidics.* **2021**, *25*, 1.
[20] K. Samlali, C. L. Alves, M. Jezernik, S. C. C. Shih, *Microsyst. Nanoeng.* **2022**, *8*, 123.
[21] A. M. Pit, R. de Ruiter, A. Kumar, D. Wijnperlé, M. H. G. Duits, F. Mugele, *Biomicrofluidics.* **2015**, *9*, 044116.
[22] F. Ahmadi, K. Samlali, P. Q. N. Vo, S. C. C. Shih, *Lab Chip.* **2019**, *19*, 524.
[23] F. Ahmadi, H. Tran, N. Letourneau, S. R. Little, A. Fortin, A. N. Moraitis, S. C. C. Shih, *Small.* **2024**, *20*, 2308950.
[24] M. Novo, R. Gonzalez, E. Bertran, M. Martínez, M. Yuste, P. Morales, *LWT – Food Sci. Technol.* **2014**, *58*, 166.
[25] K. Samlali, F. Ahmadi, A. B. V. Quach, G. Soffer, S. C. C. Shih, *Small.* **2020**, *16*, 2070190.
[26] J. J. Agresti, E. Antipov, A. R. Abate, K. Ahn, A. C. Rowat, J. C. Baret, M. Marquez, A. M. Klibanov, A. D. Griffiths, D. A. Weitz, *Proc. Natl. Acad. Sci. U. S. A.* **2010**, *107*, 4004.
[27] S. Neun, P. Brear, E. Campbell, T. Tryfona, K. El Omari, A. Wagner, P. Dupree, M. Hyvönen, F. Hollfelder, *Nat. Chem. Biol.* **2022**, *18*, 1096.
[28] C. Leal-Alves, Z. Deng, N. Kermeci, S. C. C. Shih, *Lab Chip.* **2024**, *24*, 2834.
[29] H. Zhang, A. R. Guzman, J. A. Wippold, Y. Li, J. Dai, C. Huang, A. Han, *Lab Chip.* **2020**, *20*, 3948.
[30] A. Saint-Sardos, S. Sart, K. Lippera, E. Brient-Litzler, S. Michelin, G. Amselem, C. N. Baroud, *Small.* **2020**, *16*, e2002303.
[31] I. C. Clark, C. L. Delley, C. Sun, R. Thakur, S. L. Stott, S. Thaploo, Z. Li, F. J. Quintana, A. R. Abate, *Anal. Chem.* **2020**, *92*, 14616.
[32] H. Zhang, C. Huang, Y. Li, R. Gupte, R. Samuel, J. Dai, A. Guzman, R. Sabnis, P. de Figueiredo, A. Han, *Sci. Adv.* **2022**, *8*, eabc9108.
[33] R. Gan, M. D. Cabezas, M. Pan, H. Zhang, G. Hu, L. G. Clark, M. C. Jewett, R. Nicol, *ACS Synth. Biol.* **2022**, *11*, 2108.
[34] A. Gérard, A. Woolfe, G. Mottet, M. Reichen, C. Castrillon, V. Menrath, S. Ellouze, A. Poitou, R. Doineau, L. Briseno-Roa, P. Canales-Herrerias, P. Mary, G. Rose, C. Ortega, M. Delincé, S. Essono, B. Jia, B. Iannascoli, O. Richard-Le Goff, R. Kumar, S. N. Stewart, Y. Pousse, B. Shen, K. Grosselin, B. Saudemont, A. Sautel-Caillé, A. Godina, S. McNamara, K. Eyer, G. A. Millot, et al., *Nat. Biotechnol.* **2020**, *38*, 715.
[35] T. Beneyton, I. P. M. Wijaya, P. Postros, M. Najah, P. Leblond, A. Couvent, E. Mayot, A. D. Griffiths, A. Drevelle, *Sci. Rep.* **2016**, *6*, 27223.
[36] K. Krogerus, B. Gibson, *Appl. Microbiol. Biotechnol.* **2020**, *104*, 3745.
[37] J. Nemenyi, E. R. Pitts, A. Martin-Ryals, Z. Boz, B. Zhang, Z. Jia, D. Budner, A. J. MacIntosh, K. A. Thompson-Witrick, *J. Food Sci.* **2024**, *89*, 513.
[38] X. Zong, L. Wen, Y. Wang, L. Li, *J. Food Biochem.* **2022**, *46*, e14099.
[39] R. A. Cripwell, R. My, L. Treu, S. Campanaro, L. Favaro, W. H. van Zyl, M. Viljoen-Bloom, *Bioresour. Technol.* **2023**, *388*, 129787.
[40] T. Meier-Dörnberg, O. I. Kory, F. Jacob, M. Michel, M. Hutzler, *FEMS Yeast Res.* **2018**, *18*, 1.
[41] S. Neun, L. van Vliet, F. Hollfelder, F. Gielen, *Anal. Chem.* **2022**, *94*, 16701.
[42] F. Gielen, R. Hours, S. Emond, M. Fischlechner, U. Schell, F. Hollfelder, *Proc. Natl. Acad. Sci. U. S. A.* **2016**, *113*, E7383.
[43] R. He, R. Ding, J. A. Heyman, D. Zhang, R. Tu, *J. Ind. Microbiol. Biotechnol.* **2019**, *46*, 1603.
[44] D. Mangan, A. Draga, R. Ivory, C. Cornaggia, M. Blundell, C. Howitt, B. McCleary, J. P. Ral, *J. Cereal Sci.* **2022**, *105*, 103480.
[45] T. Luthra, R. Agarwal, M. Estari, U. Adepally, S. Sen, *Sci. Rep.* **2017**, *7*, 13246.
[46] X. Zhu, B. Arman, J. Chu, Y. Wang, Y. Zhuang, *Biotechnol. Lett.* **2017**, *39*, 739.
[47] H. Zhang, H. Kallwass, S. P. Young, C. Carr, J. Dai, P. S. Kishnani, D. S. Millington, J. Keutzer, Y.-T. Chen, D. Bali, *Genet. Med.* **2006**, *8*, 302.
[48] C. I. Soares Rodrigues, M. den Ridder, M. Pabst, A. K. Gombert, S. A. Wahl, *Sci. Rep.* **2023**, *13*, 2126.
[49] Ö. Kayikci, J. Nielsen, *FEMS Yeast Res.* **2015**, *15*, fov068.
[50] M. Parapouli, A. Vasileiadis, A.-S. Afendra, E. Hatziloukas, *AIMS Microbiol.* **2020**, *6*, 1.
[51] M. Gomar-Alba, M. Á. Morcillo-Parra, M. del Olmo, *FEMS Yeast Res.* **2015**, *15*, fov039.
[52] S. Salazar-Cerezo, R. P. de Vries, S. Garrigues, *J. Fungi.* **2023**, *9*, 834.
[53] J. Kellershohn, I. Russell, in *Advances in Food Biotechnology*, John Wiley & Sons Ltd, New Jersey, USA **2015**, pp. 303–310.
[54] J. Steensels, T. Snoek, E. Meersman, M. Picca Nicolino, E. Aslankoohi, J. F. Christiaens, R. Gemayel, W. Meert, A. M. New, K. Pougach, V. Saels, E. van der Zande, K. Voordeckers, K. J. Verstrepen, *Cerevisia.* **2012**, *37*, 63.
[55] J.-J. Liu, W.-T. Ding, G.-C. Zhang, J.-Y. Wang, *Appl. Microbiol. Biotechnol.* **2011**, *91*, 1239.
[56] T. D Abt, B. Souffriau, M. R. Foulquié-Moreno, J. Duitama, J. M. Thevelein, *Microb. Cell.* **2016**, *3*, 159.
[57] Y. Su, W. Shao, A. Zhang, W. Zhang, *FEMS Yeast Res.* **2021**, *21*, foab012.
[58] T. H. Yoo, M. Pogson, B. L. Iverson, G. Georgiou, *ChemBioChem.* **2012**, *13*, 649.
[59] M. Wehrs, A. de Beaumont-Felt, A. Goranov, P. Harrigan, S. de Kok, S. Lieder, J. Vallandingham, K. Tyner, *J. Ind. Microbiol. Biotechnol.* **2020**, *47*, 913.
[60] D. Biot-Pelletier, D. Pinel, K. Larue, V. J. J. Martin, *Biotechnol. Biofuels.* **2018**, *11*, 282.
[61] J. James, S. Towers, J. Foerster, H. Steel, *bioRxiv.* **2024**, https://doi.org/10.1101/2024.03.18.585521.
[62] N. R. Wright, M. M. Jessop-Fabre, B. J. Sánchez, T. Wulff, C. T. Workman, N. P. Rønnest, N. Sonnenschein, *Appl. Environ. Microbiol.* **2022**, *88*, e0230721.
[63] A. D. McDonald, P. M. Higgins, A. R. Buller, *Nat. Commun.* **2022**, *13*, 5242.
[64] J. Hira, B. Singh, T. Halder, A. Mahmutovic, C. Ajayi, A. A. Sekh, K. Hegstad, M. Johannessen, C. S. Lentz, *Commun Biol.* **2024**, *7*, 1228.
[65] J. S. Yu, D. A. Pertusi, A. V Adeniran, K. E. J. Tyo, *Bioinformatics.* **2016**, *33*, 909.
[66] D.-Q. Zheng, J. Chen, K. Zhang, K.-H. Gao, O. Li, P.-M. Wang, X.-Y. Zhang, F.-G. Du, P.-Y. Sun, A.-M. Qu, S. Wu, X.-C. Wu, *Appl. Microbiol. Biotechnol.* **2014**, *98*, 3059.

[67] J. Steensels, T. Snoek, E. Meersman, M. Picca Nicolino, K. Voordeckers, K. J. Verstrepen, *FEMS Microbiol. Rev.* **2014**, *38*, 947.
[68] F. W. Y. Chiu, S. Stavrakis, *Electrophoresis.* **2019**, *40*, 2860.
[69] G. Stephanopoulos, G. Locher, M. Duff, *IFAC Proc.* **1995**, *28*, 195.
[70] K. K. S. Buck, V. Subramanian, D. E. Block, *Biotechnol. Prog.* **2002**, *18*, 1366.
[71] J. C. Moore, H.-M. Jin, O. Kuchner, F. H. Arnold, *J. Mol. Biol.* **1997**, *272*, 336.
[72] M. Matukas, V. Starkute, E. Zokaityte, G. Zokaityte, D. Klupsaite, E. Mockus, J. M. Rocha, R. Ruibys, E. Bartkiene, *Foods.* **2022**, *11*, 2317.
[73] C. Laluce, J. R. Mattoon, *Appl. Environ. Microbiol.* **1984**, *48*, 17.
[74] L. Favaro, M. Basaglia, S. Casella, *Biomass Bioenergy.* **2012**, *46*, 605.
[75] E. K. Bowman, P. T. Nguyen Hoang, A. R. Gordillo Sierra, K. M. Vieira Nogueira, H. S. Alper, *Lab Chip.* **2023**, *23*, 2249.
[76] S. Li, Y. Zhang, L. Li, Y. Yuan, H. Sun, X. H. Xing, X. Wang, C. Zhang, *Biochem. Eng. J.* **2023**, *198*, 109036.
[77] M. Huang, J. Bao, B. M. Hallström, D. Petranovic, J. Nielsen, *Nat. Commun.* **2017**, *8*, 1131.
[78] L. L. B. Kastberg, R. Ard, M. K. Jensen, C. T. Workman, *Front. Fungal Biol.* **2022**, *3*, 827704.
[79] F. Li, Y. Chen, Q. Qi, Y. Wang, L. Yuan, M. Huang, I. E. Elsemman, A. Feizi, E. J. Kerkhoven, J. Nielsen, *Nat. Commun.* **2022**, *13*, 2969.
[80] J. C. de Ruijter, E. V Koskela, J. Nandania, A. D. Frey, V. Velagapudi, *Yeast.* **2018**, *35*, 331.
[81] P. Ghiaci, P. Jouhten, N. Martyushenko, H. Roca-Mesa, J. Vázquez, D. Konstantinidis, S. Stenberg, S. Andrejev, K. Grkovska, A. Mas, G. Beltran, E. Almaas, K. R. Patil, J. Warringer, *Mol. Syst. Biol.* **2024**, *20*, 1109.
[82] T. E. Sandberg, M. J. Salazar, L. L. Weng, B. O. Palsson, A. M. Feist, *Metab. Eng.* **2019**, *56*, 1.
[83] J. Mao, H. Zhang, Y. Chen, L. Wei, J. Liu, J. Nielsen, Y. Chen, N. Xu, *Biotechnol. Adv.* **2024**, *74*, 108401.
[84] S. R. Little, Z. Leung, A. B. V Quach, A. Hirukawa, F. Gholizadeh, M. Hajiaghayi, P. J. Darlington, S. C. C. Shih, *Adv. Mater. Technol.* **2023**, *8*, 2300719.
[85] M. Bahalul, G. Kaneti, Y. Kashi, *Yeast.* **2010**, *27*, 999.
[86] M. H. Shihan, S. G. Novo, S. J. Le Marchand, Y. Wang, M. K. Duncan, *Biochem Biophys Rep.* **2021**, *25*, 100916.